crystallization communications

Huijong Han[a,b] and Petri Kursula[a,b,c]*

[a]Department of Biochemistry and Biocenter Oulu, University of Oulu, Oulu, Finland, [b]Centre for Structural Systems Biology, Helmholtz Centre for Infection Research (CSSB-HZI), German Electron Synchrotron (DESY), Hamburg, Germany, and [c]Department of Chemistry, University of Hamburg, Hamburg, Germany

Correspondence e-mail: petri.kursula@oulu.fi

Preliminary crystallographic analysis of the N-terminal PDZ-like domain of periaxin, an abundant peripheral nerve protein linked to human neuropathies

Periaxin (PRX) is an abundant protein in peripheral nerves and contains a predicted PDZ-like domain at its N-terminus. The large isoform, L-PRX, is required for the maintenance of myelin in the peripheral nervous system and its defects cause neurological disease. Here, the human periaxin PDZ-like domain was crystallized and X-ray diffraction data were collected to 2.85 Å resolution using synchrotron radiation. The crystal belonged to the primitive hexagonal space group $P3_121$ or $P3_221$, with unit-cell parameters $a = b = 80.6$, $c = 81.0$ Å, $\gamma = 120°$ and either two or three molecules in the asymmetric unit. The structure of PRX will shed light on its poorly characterized function in the nervous system.
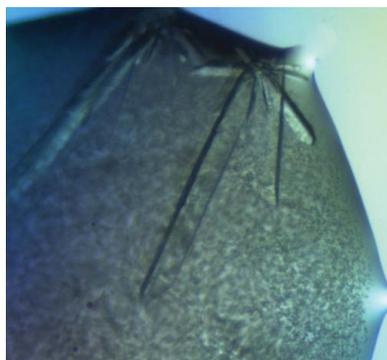
1. Introduction

Periaxin (PRX) is one of the most abundant proteins in the peripheral nervous system (PNS) myelin sheath, a membrane multilayer surrounding axons (Patzig *et al.*, 2011). PRX has two main isoforms (Fig. 1), L-PRX and S-PRX, generated by alternative mRNA splicing (Dytrych *et al.*, 1998). L-PRX is expressed at the early stages of PNS development and distributes first to the adaxonal plasma membrane and then to the abaxonal plasma membrane, while S-PRX is located evenly throughout the cytoplasm as well as in the nucleus of the Schwann cell (Gillespie *et al.*, 1994; Scherer *et al.*, 1995; Dytrych *et al.*, 1998).

To date, the functions of PRX at the molecular level remain unclear. It is assumed that L-PRX is involved in the stabilization of myelin in the PNS (Gillespie *et al.*, 1994). Genetic defects in L-PRX cause demyelinating peripheral neuropathies, such as Charcot–Marie–Tooth (CMT4F) and Dejerine–Sottas diseases (Takashima *et al.*, 2002), indicating that an abnormality in L-PRX structure and function results in nerve damage. The disease-related mutations that have been characterized generally result in C-terminally truncated periaxin.

Both PRX isoforms have their 127 N-terminal amino acids in common, including a segment with sequence homology to PDZ (PSD-95, Discs large, ZO-1) domains. Outside this common domain, the PRX isoforms are predicted to be largely disordered (Han *et al.*, 2013). PDZ domains are among the most common protein–protein-interacting modules and they play an important role in the organization of signalling complexes (Ivarsson, 2012). PDZ domains bind to the C-termini of target proteins or to internal peptide motifs (Saras & Heldin, 1996; Cowburn, 1997). The ligands are usually transmembrane receptors or ion channels. Hence, PDZ-containing proteins are typically involved in the assembly of supramolecular complexes that play roles in signalling at specific subcellular locations. Individual PDZ domains consist of 80–100 amino acids and more than 200 PDZ domain structures are currently available in the PDB.

Through its interactions with the dystrophin-related protein 2 (Drp2), L-PRX is a member of the periaxin–Drp2–dystroglycan complex. It has been proposed that the L-PRX basic domain, located C-terminal to the PDZ domain, interacts with Drp2 (Sherman *et al.*,

Table 1
Recombinant periaxin production information.

In the primers, the position of the engineered stop codon is shown in bold. In addition, in the protein sequence the His tag and the TEV protease cleavage site are indicated in bold.

Source organism	*Homo sapiens*
DNA source	Synthetic gene
Deletion primer 1	5′-ATCTTTATTTTCAGGGCGCAGAACTGGTCG-AGATTAT-3′
Deletion primer 2	5′-TCTCGACCAGTTCTGCGCCCTGAAAATAAA-GATTCTC-3′
Mutagenesis primers	
128-to-stop forward	5′-GCGAAAGTCGCGAAACTC**TAG**CGCGTGTT-GAGCCCAGC-3′
128-to-stop reverse	5′-GCTGGGCTCAACACGCG**CTA**GAGTTTCGC-GACTTTCGC-3′
18-to-stop forward	5′-CGGGCTATGAGATC**TAA**GGGCCTCGTGCG-3′
118-to-stop reverse	5′-CGCACGAGGCCC**TTA**GATCTCATAGCCCG-3′
108-to-stop forward	5′-GACTGGAGACTTAGCCCTT**TAG**CCTGGTAC-GGTATCGGG-3′
108-to-stop reverse	5′-CCCGATACCGTACCAGG**CTA**AAGGGCTAAG-TCTCCAGTC-3′
Expression vector	pETM11
Expression host	*E. coli* Rosetta(DE3)
Complete amino-acid sequence of the construct PRX14-107	MK**HHHHHH**PMSDYDIPTT**ENLYFQ/G**A(14)ELV-EIIVETEAQTGVSGINVAGGGKEGIFVRELRE-DSPAARSLSL QEGDQLLSARVFFENFKYEDA-LRLLQCAEPYKVSFCLKRTVPTGDLAL(107)

2001). However, ligands for the PDZ homology domain in PRX have not yet been discovered.

Here, we present the successful recombinant production of the PDZ-like domain of PRX; an X-ray diffraction data set was obtained from a single crystal. Further efforts towards structure determination are ongoing, and the result will yield the first structure of any domain of PRX and eventually help in understanding its function. In addition, as the sequence identity of PRX to PDZ domains of known structure is very low, the structure may reveal novel aspects of PDZ-domain structure.

2. Materials and methods

2.1. Expression-construct preparation and recombinant periaxin production

A codon-optimized synthetic gene of human S-PRX (accession No. AAK19280; locus tag AF321192_1), subcloned into the pETM11 expression vector, was purchased from Eurofins MWG Operon. The construct contains a hexahistidine tag and a *Tobacco etch virus* (TEV) protease cleavage site, followed by full-length human S-PRX (residues 1–147). Shorter constructs, containing PRX residues 14–127, 14–117 or 14–107, were generated by a deletion reaction using Platinum *Taq* High Fidelity DNA polymerase (Invitrogen) (to

Table 2
Crystallization details.

|	
Method	Sitting-drop vapour diffusion
Plate type	Swissci MRC plate
Temperature (K)	293
Protein concentration (mg ml^{-1})	33
Buffer composition of protein solution	50 mM Tris pH 7.5, 100 mM NaCl
Composition of reservoir solution	30%(w/v) PEG 2000 MME, 0.15 M KBr
Volume and ratio of drop	0.3 µl protein + 0.3 µl reservoir
Volume of reservoir (µl)	50

shorten the N-terminus) and mutagenesis using the QuikChange Lightning site-directed mutagenesis kit (Agilent Technologies) (to insert stop codons at selected C-terminal sites). The primers for the deletion and mutagenesis reactions are listed in Table 1.

The recombinant PRX variants were expressed in *Escherichia coli* Rosetta(DE3) cells in auto-inducible ZY-5052 medium (Studier, 2005) containing 50 µg ml^{-1} kanamycin and 34 µg ml^{-1} chloramphenicol. The cells were grown at 293 K for 20 h and harvested by centrifugation. The cell pellets were resuspended in 10 ml lysis buffer (50 mM Tris pH 7.5, 100 mM NaCl) per gram of cell pellet and lysed by sonication. The soluble fraction was separated from debris by centrifugation at 14 500g for 1 h at 277 K.

The supernatant was loaded onto an Ni–NTA gravity column pre-equilibrated with lysis buffer containing 20 mM imidazole. Unbound proteins were washed out with five column volumes of the same buffer and the bound proteins were eluted with lysis buffer containing 500 mM imidazole. The buffer of the eluate was exchanged back to the lysis buffer using a PD-10 column (GE Healthcare). The protein concentration was measured based on the absorbance at 280 nm, and a 1:10(w:w) ratio of His-tagged TEV protease (van den Berg *et al.*, 2006) was added. The cleavage reaction was carried out at 277 K overnight. On the next day, the reaction mixture was again mixed with Ni–NTA resin in a gravity column and the flowthrough and five column volumes of washing fractions were collected. To obtain monodisperse protein and to remove remaining impurities, size-exclusion chromatography was performed using a Superdex 75 10/300 GL column (GE Healthcare), eluting with the lysis buffer. The fractions corresponding to the main peak were pooled and concentrated to 25–36 mg ml^{-1} by centrifugal ultra-filtration using VivaSpin devices with a 5 kDa molecular-weight cutoff (Sartorius).

2.2. Crystallization

Crystallization screening was performed by the sitting-drop vapour-diffusion method using the commercially available JCSG+ (Molecular Dimensions), Crystal Screen 2 and PEG/Ion (Hampton
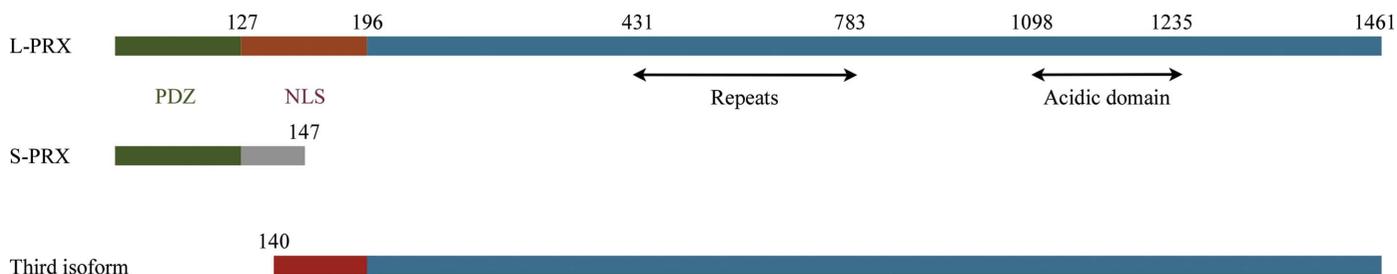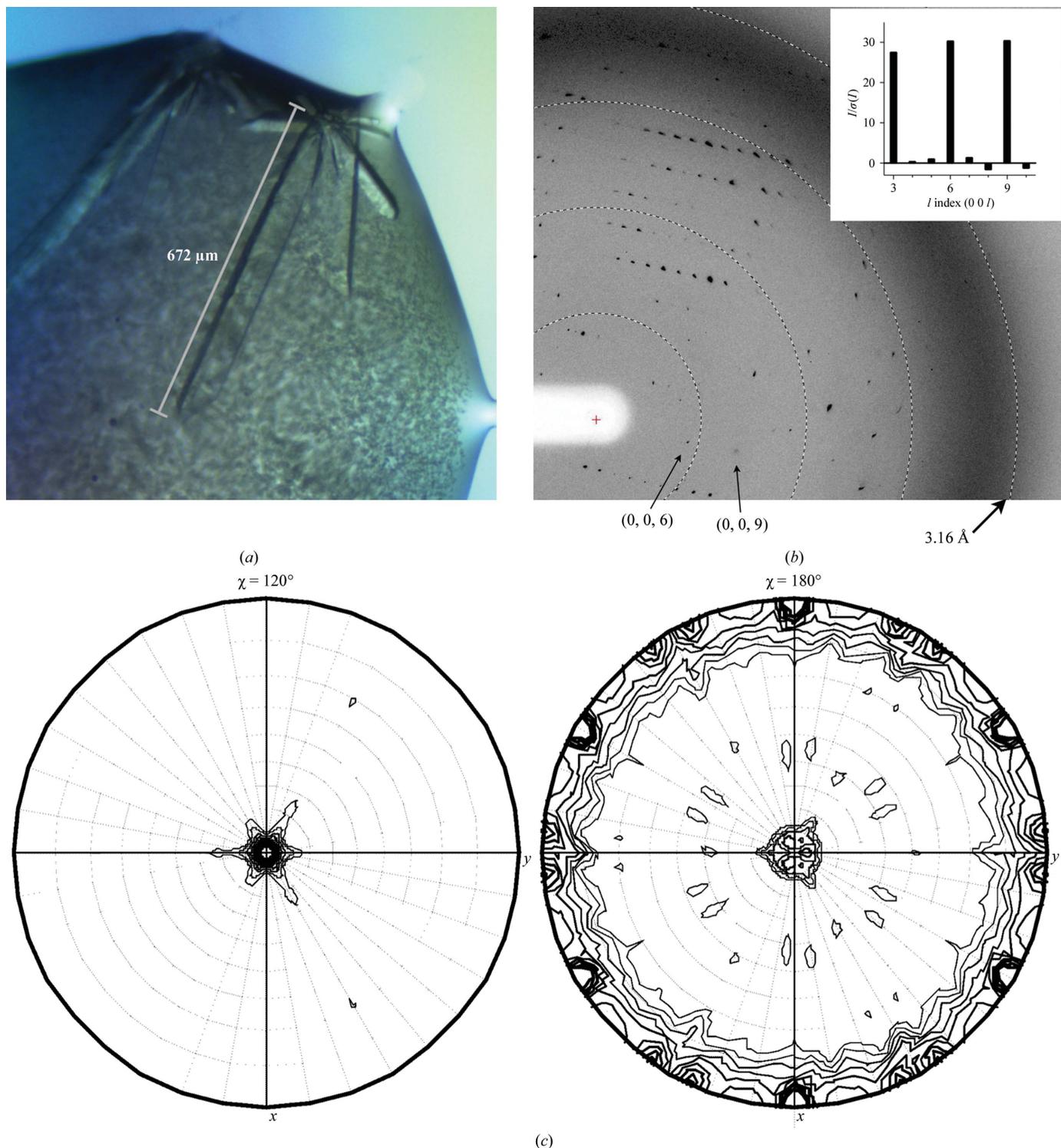

Figure 1
The classical PRX isoforms include large (L-PRX) and small (S-PRX) periaxin; in addition, a sequence for a third isoform can be found in sequence databases. The locations of the PDZ domain and the nuclear localization signal (NLS)/basic domain, as well as the repeat and acidic domains, are indicated.

Research) screens. Drops were prepared by adding 0.3 µl protein solution to an equal volume of reservoir solution and the mixture was equilibrated against 50 µl reservoir solution in a 96-well plate at 293 K. Initial crystals formed after overnight incubation.

Crystallization conditions were further optimized by modifying the protein and precipitant concentration, the salt and the incubation temperature. Details of the crystallization protocol are given in Table 2.

Figure 2
Diffraction analysis of PRX crystals. (*a*) Crystals of PRX14–107 formed in 30% PEG 2000 MME and 0.15 *M* KBr. The trigonal rods have a maximum dimension of 0.7 mm. (*b*) Diffraction pattern from the crystal used for data collection. The resolution ring at 3.16 Å is marked. Systematic absences clearly indicate the presence of a threefold screw axis (inset). (*c*) Self-rotation function calculated by *MOLREP* (Vagin & Teplyakov, 2010). In addition to the crystallographic peaks, a twofold self-rotation peak is detectable at $\theta = 90°$, $\varphi = -24.5°$.
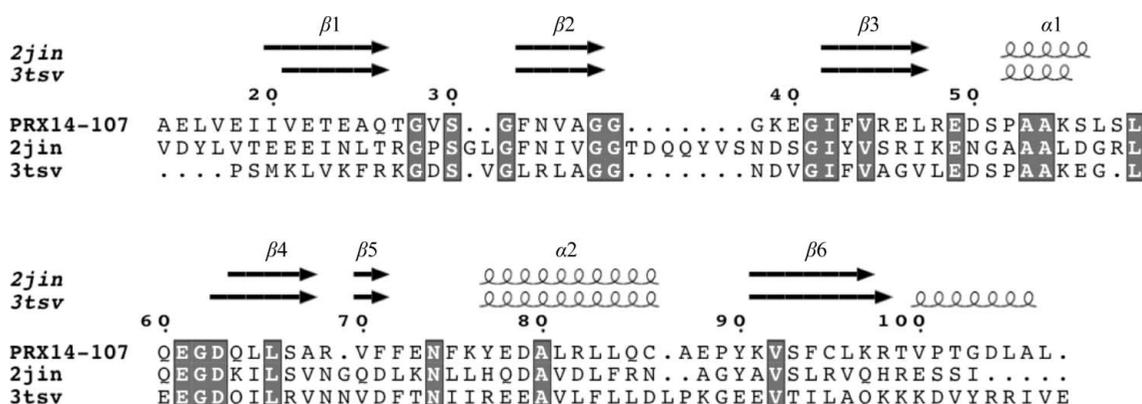
Figure 3
Sequence alignment, prepared using *ClustalW* (Thompson *et al.*, 1994) and *ESPript* (Gouet *et al.*, 1999), of PRX with two of its closest sequence homologues in the PDB: PDZ domains from the human synaptojanin-2 binding protein (PDB entry 2jin; J. Tickle, C. Phillips, A. C. W. Pike, C. Cooper, E. Salah, J. Elkins, A. P. Turnbull, A. Edwards, C. H. Arrowsmith, J. Weigelt, M. Sundstrom & D. Doyle, unpublished work) and the human zonula occludens membrane-associated guanylate kinase protein ZO-1 (PDB entry 3tsv; Nomme *et al.*, 2011). Identical residues are shaded and secondary structures from the two known structures are shown above the alignment.

Table 3
Data collection and processing.

Values in parentheses are for the outer shell.

Diffraction source	I911-3, MAX-lab
Wavelength (Å)	1.0
Temperature (K)	100
Detector	MAR Mosaic 225
Crystal-to-detector distance (mm)	280
Rotation range per image (°)	0.5
Total rotation range (°)	72.5
Exposure time per image (s)	10
Space group	$P3_121$ or $P3_221$
Unit-cell parameters (Å, °)	$a = b = 80.6$, $c = 81.0$,
	$\alpha = \beta = 90$, $\gamma = 120$
Resolution range (Å)	30–2.85 (2.92–2.85)
Total No. of reflections	32276
No. of unique reflections	7396
Completeness (%)	99.4 (99.8)
Multiplicity	4.4 (4.5)
$\langle I/\sigma(I)\rangle$†	20.1 (1.3)
R_{meas}‡	0.051 (1.055)
$CC_{1/2}$§ (%)	99.9 (62.5)
Overall B factor from Wilson plot (Å²)	80

† The mean $I/\sigma(I)$ in the outer shell falls below 2.0 at approximately 2.95 Å resolution. ‡ R_{meas} is the redundancy-independent merging R factor, as defined by Diederichs & Karplus (1997) and Weiss & Hilgenfeld (1997). $R_{meas} = \sum_{hkl}\{N(hkl)/[N(hkl)-1]\}^{1/2}\sum_i|I_i(hkl) - \langle I(hkl)\rangle|/\sum_{hkl}\sum_i I_i(hkl)$. § $CC_{1/2}$ is defined as the correlation coefficient between two random half data sets, as described by Karplus & Diederichs (2012).

2.3. Data collection and processing

X-ray diffraction data were collected using synchrotron radiation on beamline I911-3 at MAX-lab, Lund, Sweden (Ursby *et al.*, 2004). A single crystal of PRX14-107 was picked up into a LithoLoop (Molecular Dimensions) and directly flash-cooled in liquid nitrogen. Diffraction data were collected to 2.85 Å resolution and the data were processed using *XDS* (Kabsch, 2010). Data-processing statistics and further details of data collection are given in Table 3.

3. Results and discussion

The recombinant PRX constructs containing the predicted PDZ-like domain could be overexpressed and purified in soluble form on a large scale. The yield of pure protein from 1 l bacterial culture varied between 5 and 50 mg depending on the construct. Crystals were formed at high concentrations of PRX14–127, PRX14–117 and PRX14–107, and the best crystals were grown with the PRX14–107 construct in a condition consisting of 30% PEG 2000 MME and 0.15 *M* KBr with no additional buffering (Fig. 2). The size of the largest crystal reached 0.7 mm in one direction, while the other edges grew to 0.05 mm.

The collected diffraction data were processed to 2.85 Å resolution (Fig. 2). The data statistics are summarized in Table 3. The space group could be determined to be either $P3_121$ or $P3_221$, with unit-cell parameters $a = b = 80.6$, $c = 81.0$ Å, $\gamma = 120°$. The calculated Matthews coefficient (Matthews, 1968) suggested three monomers per asymmetric unit (V_M of 2.46 Å³ Da⁻¹, corresponding to a solvent content of 50%), although the presence of only two monomers could also be possible (V_M 3.69 Å³ Da⁻¹, solvent content 67%; Matthews, 1968). The data presented no signs of twinning or translational pseudosymmetry (data not shown). A self-rotation function calculated from the data indicated twofold noncrystallographic symmetry (Fig. 2), which suggests the presence of a dimer in the asymmetric unit.

Molecular-replacement trials have so far failed in our hands using several different programs and a number of search models, including both experimental and modelled structures. The sequence identity of the PRX PDZ-like domain to other PDZ domains with known structure is very low, which explains the failure of molecular-replacement approaches (Fig. 3). The PRX crystallization condition contained bromide ions, but the anomalous signal was weak and attempts at phasing by single-wavelength anomalous diffraction (SAD) also failed.

Owing to the difficulty of phasing with our current PRX diffraction data, experimental phasing using different heavy atoms is currently under way. We anticipate that determination of the three-dimensional structure of the PRX PDZ-like domain will contribute centrally to the elucidation of the function of PRX in the nervous system and will fill an important gap in the structural biology of vertebrate myelin.

References

van den Berg, S., Löfdahl, P. A., Härd, T. & Berglung, H. (2006). *J. Biotechnol.* **121**, 291–298.
Cowburn, D. (1997). *Curr. Opin. Struct. Biol.* **7**, 835–838.

crystallization communications

Diederichs, K. & Karplus, P. A. (1997). *Nature Struct. Biol.* **4**, 269–275.

Dytrych, L., Sherman, D. L., Gillespie, C. S. & Brophy, P. J. (1998). *J. Biol. Chem.* **273**, 5794–5800.

Gillespie, C. S., Sherman, D. L., Blair, G. E. & Brophy, P. J. (1994). *Neuron*, **12**, 497–508.

Gouet, P., Courcelle, E., Stuart, D. I. & Métoz, F. (1999). *Bioinformatics*, **15**, 305–308.

Han, H., Myllykoski, M., Ruskamo, S., Wang, C. & Kursula, P. (2013). *BioFactors*, **39**, 233–241.

Ivarsson, Y. (2012). *FEBS Lett.* **586**, 2638–2647.

Kabsch, W. (2010). *Acta Cryst.* D**66**, 125–132.

Karplus, P. A. & Diederichs, K. (2012). *Science*, **336**, 1030–1033.

Matthews, B. W. (1968). *J. Mol. Biol.* **33**, 491–497.

Nomme, J., Fanning, A. S., Caffrey, M., Lye, M. F., Anderson, J. M. & Lavie, A. (2011). *J. Biol. Chem.* **286**, 43352–43360.

Patzig, J. *et al.* (2011). *J. Neurosci.* **31**, 16369–16386.

Saras, J. & Heldin, C. H. (1996). *Trends Biochem. Sci.* **21**, 455–458.

Scherer, S. S., Xu, Y. T., Bannerman, P. G., Sherman, D. L. & Brophy, P. J. (1995). *Development*, **121**, 4265–4273.

Sherman, D. L., Fabrizi, C., Gillespie, C. S. & Brophy, P. J. (2001). *Neuron*, **30**, 677–687.

Studier, F. W. (2005). *Protein Expr. Purif.* **41**, 207–234.

Takashima, H., Boerkoel, C. F., de Jonghe, P., Ceuterick, S., Martin, J. J., Voit, T., Schröder, J. M., Williams, A., Brophy, P. J., Timmerman, V. & Lupski, J. R. (2002). *Ann. Neurol.* **51**, 709–715.

Thompson, J. D., Higgins, D. G. & Gibson, T. J. (1994). *Nucleic Acids Res.* **22**, 4673–4680.

Ursby, T., Mammen, C. B., Cerenius, Y., Svensson, C., Sommarin, B., Fodje, M. N., Kvick, Å., Logan, D. T., Als-Nielsen, J. & Thunnissen, M. M. G. M. (2004). *AIP Conf. Proc.* **705**, 1241–1246.

Vagin, A. & Teplyakov, A. (2010). *Acta Cryst.* D**66**, 22–25.

Weiss, M. S. & Hilgenfeld, R. (1997). *J. Appl. Cryst.* **30**, 203–205.